

Diagonalizing large-scale quantum many-body Hamiltonians using variational quantum circuit and tensor network

Peng-Fei Zhou,¹ Shuang Qiao,¹ An-Chun Ji,¹ and Shi-Ju Ran^{1,*}

¹*Center for Quantum Physics and Intelligent Sciences,
Department of Physics, Capital Normal University, Beijing 10048, China*

(Dated: August 11, 2025)

Exact diagonalization (ED) is an essential tool for exploring quantum many-body physics but is fundamentally limited by the exponentially-scaled computational complexity. Here, we propose tensor network variational diagonalization (TNVD), which encodes the full eigenenergy spectrum of a quantum many-body Hamiltonian into a matrix product state, and encodes the eigenstates as the evolutions of product states using variational quantum circuit (VQC). Thereby, TNVD reduces the computational complexity of diagonalization from exponential to polynomial in system size N . Numerical benchmarks up to $N = 100$ spins are provided, which far surpass the computational limit of ED. We further consider quantum Ising model in a random field to reveal the underlying reliance between the efficiency of TNVD and entanglement properties of eigenstates. Typical signs, including the distribution of entanglement entropy (EE) versus eigenenergy and the density of state versus EE, are suggested to indicate area law of entanglement entropy or its violation, which are essential to the TNVD efficiency. Our work establishes TNVD as a powerful and scalable diagonalization approach for large-scale quantum many-body Hamiltonians. The incorporation of VQC lays a promising pathway to applying quantum computation to address the volume-law-EE Hamiltonians that lack efficient classical approaches.

Introduction.— The eigenenergy spectra of quantum many-body Hamiltonians encode not only equilibrium characteristics but also the full structure of quantum dynamics. They underpin our understanding of criticality, phase transitions. Analytical methods, such as Bethe ansatz [1, 2], provide invaluable exact solutions but are inapplicable to generic non-integrable systems. Exact diagonalization (ED) computes the complete spectrum for small-size systems, making it a fundamental tool with wide applications in, e.g., thermalization, quantum chaos, and eigenstate entanglement [3–5]. However, the computational cost of ED in general scales exponentially with the system size, which is known as the “exponential wall”, severely limiting its applicability. Taking interacting spin systems as examples, the sizes that ED can access are generally less than 30 spins, even after exploiting symmetries of the Hamiltonians [6–8].

Tremendous efforts have been made to access the eigenenergies and eigenstates of large-scale quantum many-body Hamiltonians. Among others, density matrix renormalization group (DMRG) [9, 10] and its variants [11–14] can efficiently simulate the eigenenergies and eigenstates of large quantum many-body systems, but are limited to a small part of the eigenstates, say the low-lying eigenstates or the scar states. More recently, inspiring progress has been made in developing variational diagonalization methods, such as variational unitary matrix product operator ansatz [15, 16]. Still, efficient diagonalization approaches with polynomial complexity in system size are strongly desired,

In this work, we aim to tackle the “exponential wall” in diagonalizing quantum many-body Hamiltonians by proposing an efficient diagonalization approach named tensor network variational diagonalization (TNVD). Our key idea is encoding the full eigenenergy spectrum of the Hamiltonian into a matrix product state (MPS), and meanwhile encodes the eigenstates as the evolutions of product states using variational quantum

circuit (VQC) [17, 18], thereby reducing the computational complexity of diagonalization from exponential to polynomial in system size N . Our benchmarks demonstrate high efficiency in diagonalizing quantum spin systems of sizes up to $N = 100$, which far surpass the computational limit of ED and the existing variational approaches[15, 16, 19–21]. The computational error can be well controlled by a logarithmic Schmidt distance [22] that can be simulated classically with high efficiency.

We further reveal the underlying relation between TNVD efficiency and the entanglement properties of eigenstates by considering quantum Ising model in a random longitudinal field as an example. Our results suggest high accuracy of TNVD in the standard and deep many-body localized phases [23–28], where the entanglement entropy (EE) of eigenstates are deemed to obey the area law [29–32]. Within the thermalized phase [33, 34], our results imply two sub-regions: a transition sub-region from area-law to volume-law EE, and a sub-region exhibiting volume-law EE. Numerical evidences and typical signs, including the errors of TNVD, distribution of EE versus eigenenergy, and density of states versus EE, are suggested, which allow to assess the strength of eigenstate entanglement and TNVD efficiency.

Tensor network variational diagonalization approach.— Considering a quantum system of N spin-1/2’s, the eigenvalue decomposition of its Hamiltonian \hat{H} is given by

$$\hat{H} = \sum_{\alpha=0}^{2^N-1} E_\alpha |\alpha\rangle\langle\alpha|, \quad (1)$$

where $\{E_\alpha\}$ form the eigenenergy spectrum and $\{|\alpha\rangle\}$ represent the eigenstates satisfying $\hat{H}|\alpha\rangle = E_\alpha|\alpha\rangle$. The index α can be expressed in the binary form as $\alpha \equiv (r_1, r_2, \dots, r_N)$ with $r_m = 0$ or 1 . Then we write $|\alpha\rangle$ as the evolution by the unitary transformation \hat{U} on the product state $\{|r_\alpha\rangle\equiv$

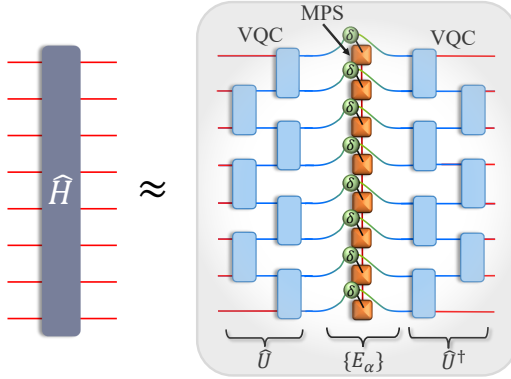


FIG. 1. (Color online) Illustration of TNVD ansatz encoding of the eigenvalue decomposition of a given Hamiltonian [Eq. (1)]. The exponentially-many eigenenergies $\{E_\alpha\}$ are encoded into an MPS. The eigenstates are encoded into the evolutions of VQC on product states as $|\alpha\rangle = \hat{U}|r_\alpha\rangle$. The ansatz is formed by the MPS and VQC (and its conjugate) connected by super-diagonal tensors.

$|r_1 r_2 \cdots r_N\rangle\}$ as $|\alpha\rangle = \hat{U}|r_\alpha\rangle$.

By treating the eigenenergy spectrum as an N th-order tensor $E_{r_1 r_2 \cdots r_N}$, we encode it into an MPS as

$$E_{r_1 \cdots r_N} = \sum_{a_1 \cdots a_N} \left(\prod_{n=1}^N A_{r_n a_n a_{n+1}}^{[n]} \right), \quad (2)$$

with $\{A^{[n]}\}$ the local tensors (see the yellow squares in Fig. 1) and $\{a_n\}$ the virtual indexes. The complexity of MPS just scales linearly with N as $O(2N\chi_a^2)$, with the virtual dimension $\chi_a = \dim(a_n)$ a hyper-parameter.

The unitary transformation \hat{U} is represented as a VQC [17, 18]. Without losing generality, we choose the “brick-wall” VQC formed by two-body gates (see the blue squares in Fig. 1). Its complexity scales as $O(NN_L)$ with N_L the VQC depth. We introduce third-order super-diagonal tensors, satisfying $\delta_{abc} = 1$ if $a = b = c$ or $\delta_{abc} = 0$ otherwise, to connect the MPS and the VQC (as well as its conjugate) [35]. The eigenvalue decomposition of \hat{H} is finally represented as a variational ansatz formed by an MPS, VQC and its conjugate, connected by N third-order super-diagonal tensors.

The local tensors of MPS and the parameters of the gates in the VQC form the variational parameters of our TNVD ansatz. We adopt latent tensors as a universal parameterization of the gates [36]. The ansatz is updated by minimizing the logarithmic Schmidt distance [22]

$$F = \log_2 |\hat{H} - \tilde{H}|^2 - N, \quad (3)$$

with \tilde{H} the Hamiltonian given by the ansatz and $|\cdot|$ the L2 norm. The variational parameters are updated using the gradient descent approach.

In computing F , we represent \hat{H} as a matrix product operator (MPO) using the *automata* scheme [37, 38], and compute $F = \log_2 [\text{Tr}(\hat{H}\hat{H}^\dagger) + \text{Tr}(\tilde{H}\tilde{H}^\dagger) - 2\text{Tr}(\hat{H}\tilde{H}^\dagger)] - N$. Inside the

logarithm term, $\text{Tr}(\hat{H}\hat{H}^\dagger)$ is the contraction of two MPO’s, which can be exactly computed with a complexity linear to N . For the second term, we exploit the unitary property of \hat{U} and have $\text{Tr}(\tilde{H}\tilde{H}^\dagger) = \sum_\alpha E_\alpha E_\alpha$, which is the inner product of two MPS’s. This can also be exactly computed with a complexity linear to N . $\text{Tr}(\hat{H}\tilde{H}^\dagger)$ can be computed by first evolving the MPO of \hat{H} with the gates in \hat{U} and \hat{U}^\dagger using time-evolving block decimation algorithm [39, 40], and then contracting the resulting MPO with the MPS’s of eigenenergies and the δ ’s. The complexity of TEBD scales as $O(N_L N \chi_t^3)$, with χ_t the dimension cut-off.

Benchmarks.— We benchmark TNVD by considering the quantum Ising chain as an example. Its Hamiltonian is written as $\hat{H} = -\sum_{n=1}^{N-1} \hat{S}_n^z \hat{S}_{n+1}^z - h \sum_{n=1}^N \hat{S}_n^x$. Taking $h = 0.2, 0.5$, and 0.8 , Fig. 2(a) demonstrates VDTN’s scalability by showing F against system size N from 6 to 100 that is far beyond the scope of ED. For $N \leq 16$ that is the accessible range by ED with our hardware at hand, we show the mean absolute error of eigenenergies

$$\epsilon = \sum_{\alpha=1}^{2^N} |E_\alpha - \tilde{E}_\alpha| / 2^N, \quad (4)$$

with $\{E_\alpha\}$ and $\{\tilde{E}_\alpha\}$ the eigenenergies obtained by ED and TNVD, respectively. Consistent trends of F and ϵ are observed, suggesting F as a valid characterization of error. For $N > 16$ where ϵ become inaccessible, F continues exhibiting sublinear growth, reaching $\sim O(10^{-1})$ for $N \rightarrow 100$, indicating controlled error for large systems. In these simulations, we take the VQC depth $N_L = 10$, the virtual dimension of the MPS $\chi_a = 8$, and the dimension cut-off in TEBD $\chi_t = 16$.

To demonstrate the validity of MPS on representing the exponentially-many eigenenergies, Fig. 2(b) shows F against the virtual dimension χ_a . Convergence is reached for about $\chi_a > 16$, suggesting that $\{E_\alpha\}$ exhibits high degree of sparsity as a tensor, which can be accurately written into an MPS with moderate χ_a . This is akin to adopting MPS to represent Schmidt coefficients of quantum many-body states [35].

Taking $N = 16$ and $h_x = 0.2$, the main panel of Fig. 2(c) shows that the low-lying eigenenergies obtained by TNVD converge to those obtained by ED as the VQC depth N_L increases. Similar observation is made for the eigenenergies at $E_\alpha \simeq 0$, as shown in the inset. These imply a VQC with moderate depth can accurately encode the eigenstates. Fig. 2(d) shows ϵ versus the eigenenergy E_α with $\epsilon \sim O(10^{-2})$ or less, suggesting excellent accuracy.

Fig. 3(a) gives the density of states N_s versus E_α for $N = 16$. Remarkable consistency between ED and TNVD is observed, where both obey the Gaussian distribution

$$f(E_n) = \frac{A}{\sigma\sqrt{2\pi}} \exp\left(-\frac{(E_n - \mu)^2}{2\sigma^2}\right), \quad (5)$$

with the standard derivative $\sigma = 1.069, 1.426, 1.910$ (ED) and $\sigma = 1.068, 1.425, 1.908$ (TNVD) for $h_x = 0.2, 0.5, 0.8$. We fix $\mu = 0$ based on the Hamiltonian symmetry.

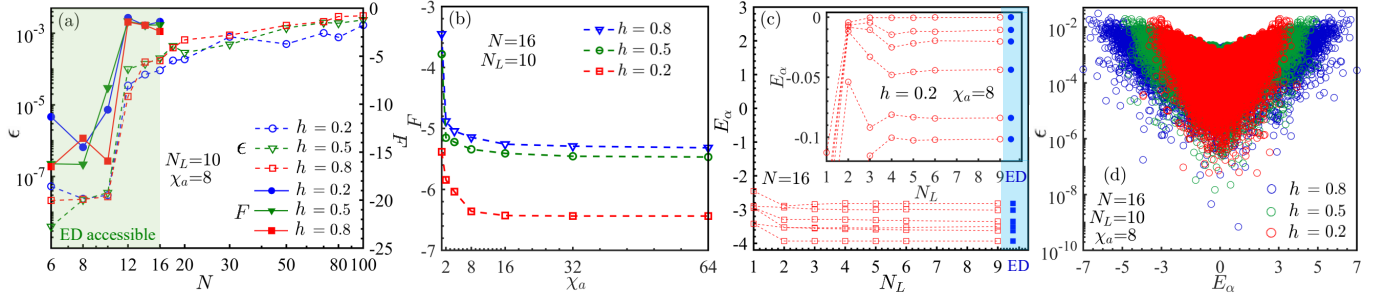


FIG. 2. (Color online) Benchmark on the quantum Ising chain. (a) The mean absolute error of eigenenergies ϵ [left y-axis; Eq. (4)] and logarithmic Schmidt distance F [right y-axis; Eq. (3)] versus the system size N . We take $h_x = 0.2, 0.5$, and 0.8 as examples. (b) F versus the virtual dimension χ_a of MPS. (c) The low-lying eigenenergies E_α converge to those obtained by ED as the VQC depth N_L increases. The inset shows the convergence of the eigenenergies for $E_\alpha \simeq 0$. (d) Distribution of ϵ with respect to the eigenenergy E_α . We take $\chi_t = 16$ in these simulations.

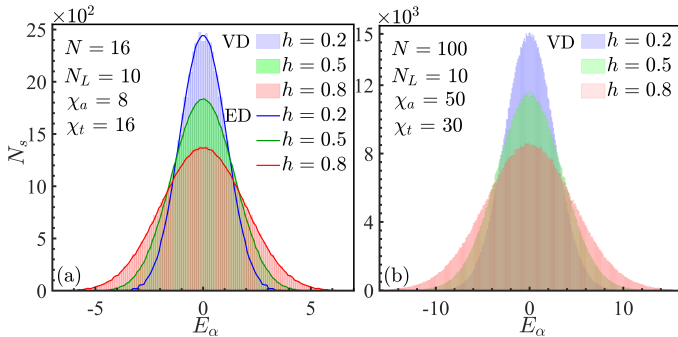


FIG. 3. (Color online) Density of states N_s against the eigenenergy E_α of the quantum Ising chain of sizes (a) $N = 16$ and (b) $N = 100$. For $N = 16$, the results obtained by ED and TNVD show remarkable consistency (see the solid lines and colored bars, respectively). Fitting the results for $h_x = 0.2, 0.5, 0.8$ by Gaussian function [Eq. (5)], we have the standard derivative $\sigma = 1.069, 1.426, 1.910$ (ED) and $\sigma = 1.068, 1.425, 1.908$ (TNVD). For $N = 100$ that is beyond the scope of ED, Gaussian distribution of N_s is also accurately obtained by TNVD with $\sigma = 2.659, 3.489, 4.676$. We fix the average $\mu = 0$ for all fittings. In (b), we randomly extract 10^6 eigenenergies, which can be done efficiently thanks to the MPS representation.

Fig. 3(b) demonstrates the N_s obtained by TNVD for $N = 100$, which is far beyond the scope of ED. The distribution accurately fulfills the Gaussian distribution with $\sigma = 2.659, 3.489, 4.676$. Notably, we here extract 10^6 eigenenergies from the full 2^{100} -dimensional eigenvalue spectrum, which is done efficiently thanks to the MPS representation. The complexity scales linearly with N . This makes a crucial advantage of TNVD comparing with the existing variational schemes [15, 16, 19–21].

Efficiency and eigenstate entanglement.— One key factor that affects the efficiency of TNVD lies in the encoding of eigenstates by VQC. Our main aim below is to uncover the relevance of TNVD efficiency to the eigenstate entanglement by considering the quantum Ising chain in a random longitude field that exhibits disorder-driven localization-thermalization-localization transitions [26, 41, 42]. The

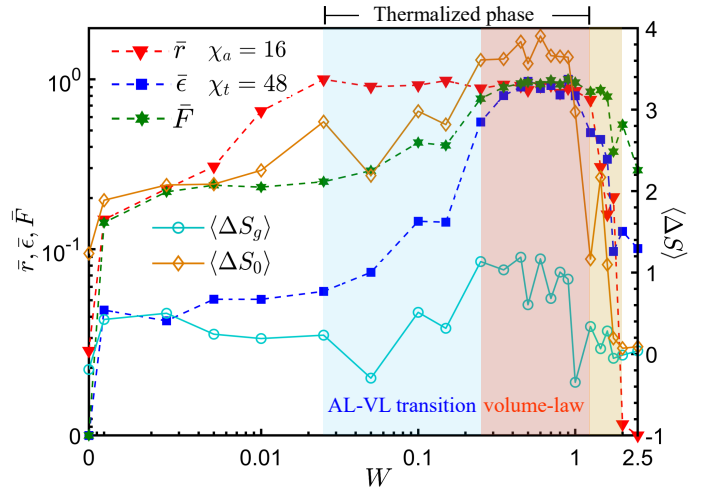


FIG. 4. (Color online) For the quantum Ising chain in a random field, we show the normalized level-spacing ratio \bar{r} , mean absolute error $\bar{\epsilon}$, and logarithmic Schmidt distance \bar{F} for the left y-axis, and the mean error of EE ($\langle \Delta S_g \rangle$ and $\langle \Delta S_0 \rangle$ for the low-lying state and the state $E_\alpha \simeq 0$, respectively) for the right y-axis, by varying the disorder strength W . The EE is simulated with the bipartition in the middle of chain, with the error obtained by comparing with ED, where we take the average on 100 low-lying eigenstates or those for $E_\alpha \sim 0$. We fix $h_x = 0.5$, $N = 14$, $N_L = 25$, $\chi_a = 16$, and $\chi_t = 48$.

Hamiltonian reads $\hat{H}^R = \hat{H} + \sum_{n=1}^N w_n \hat{S}_n^z$ with the random field $w_n \in [-W, W]$. The many-body localization (MBL) phase can be identified by the level-spacing ratio $r = \frac{1}{N_s} \sum_n \frac{\min(E_{n+1} - E_n, E_n - E_{n-1})}{\max(E_{n+1} - E_n, E_n - E_{n-1})}$, with $r \approx 0.53$ in the thermalized phases [43, 44].

Fig. 4 shows the normalized level-spacing ratio \bar{r} , mean absolute error $\bar{\epsilon}$, and logarithmic Schmidt distance \bar{F} versus the disorder strength W . By “normalized”, we mean to divide the quantity with its maximum for better illustration. The system is in the thermalized phase for $0.025 \leq W \leq 1.0$, marked by the blue and red shadows.

Two sub-regions within the thermalized phase are identified, where the TNVD error (characterized by $\bar{\epsilon}$ and \bar{F}) in-

creases with W in the first sub-region (blue) and the reaches a plateau in the second one (red). This suggests a more subtle characterization based on entanglement than r . Thus, we show the error of EE (by comparing with ED). The mean error for 100 low-lying eigenstates (denoted as $\langle \Delta S_g \rangle$) remains almost unchanged as W increases in the blue region, and exhibits just slight increase in the red region. This is speculated as a result of the EE area law that the low-lying eigenstates in a thermalized phase obey [45–48].

In contrast, the eigenstates for $E_\alpha \sim 0$ are expected to exhibit much larger EE, possibly obeying the volume law [49, 50]. The mean error $\langle \Delta S_0 \rangle$ over 100 such eigenstates increases with W in the blue region, which indicates an area-law to volume-law (AL-VL) transition. In the red region, $\langle \Delta S_0 \rangle$ forms a plateau (with certain fluctuation due to the numerical errors), which we deem as a sign of the EE volume law. After this plateau (for $W \geq 0.25$), $\langle \Delta S_0 \rangle$ drops fast as W increases, and the system is entering the deep localized phase [27, 28, 51]. The trend of $\langle \Delta S_0 \rangle$ generally coincides with those of ϵ and \bar{F} .

In Fig. 5, we further reveal the entanglement properties by showing the distribution of S versus normalized eigenenergy \bar{E}_α [see panels (a–f)] and the normalized density of state \bar{N}_s versus S [see panels (g–l)]. With a weak disorder, the system is in an MBL phase. The eigenstate EE's form a triangular distribution versus \bar{E}_α , and \bar{N}_s fits a Gaussian distribution against S [Eq. (5)]. These results imply that most of the eigenstates should exhibit area-law EE. One has the error $\epsilon \sim O(10^{-3})$.

The eigenstates transition to exhibit volume-law EE as W increases. The distribution of S converges to a slender arc [55, 56] fitted by Gaussian function. Meanwhile, \bar{N}_s exhibits a shifted Poisson distribution versus S , satisfying

$$\bar{N}_s = e^{-\frac{\Omega(\tilde{S}-S)}{\delta}}, \quad (6)$$

with \tilde{S} roughly characterizing the average amount of entanglement. By fitting, we have $\Omega = 2.864$ and $\tilde{S} = 4.233$ for $W = 0.35$ [see panel (i)]. By continue increasing W , the system enters the deep MBL phase, where the Gaussian arc of S collapses. Almost all eigenstates exhibit low EE [52–54], giving a Poisson distribution of \bar{N}_s versus S (with $\Omega = -35.6$ and $\tilde{S} = 0$ for $W = 2.5$). The error decreases to $\epsilon \sim O(10^{-3})$.

Our results suggest the “Gaussian arc” of S and shifted Poisson distribution of \bar{N}_s as the signs of volume-law EE. Meanwhile, the distribution patterns of S shown in Fig. 5 (a) and (f), and correspondingly the Gaussian and Poisson distributions of N_s shown in (g) and (l), can be regarded as the signs on high efficiency of TNVD.

Summary.— In this work, we have introduced the tensor-network variational diagonalization (TNVD), which is a scalable diagonalization approach of polynomial complexity to the system size N . The key idea is encoding the full 2^N eigenenergies of a quantum many-body Hamiltonian into a matrix product state, and encoding the eigenstates as evolu-

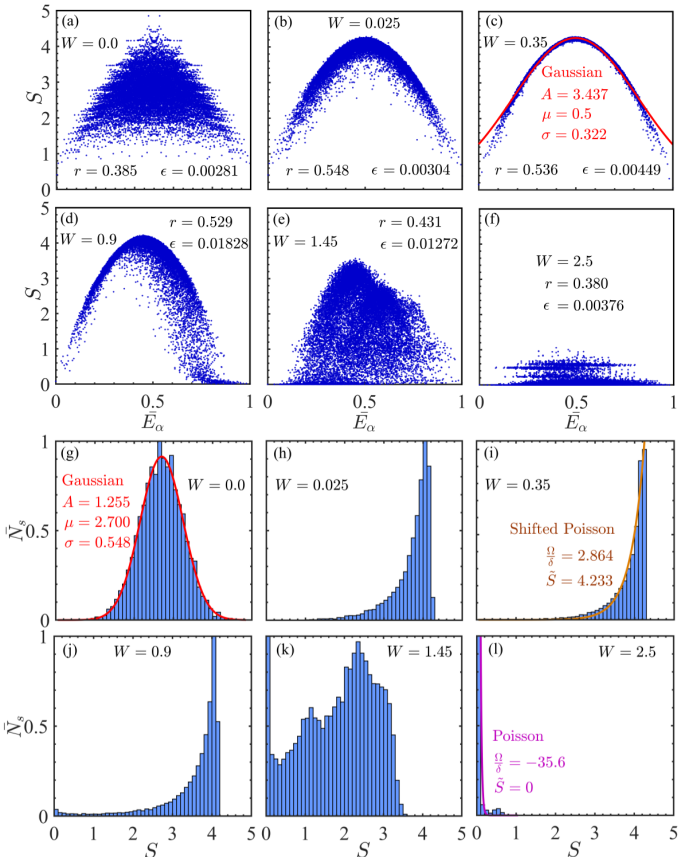


FIG. 5. (Color online) (a–f) The distribution of EE S versus normalized eigenenergy \bar{E}_α . As the disorder strength W increases, the distribution converges to a slender Gaussian arc while entering the volume-law thermalized phase, and then collapses while entering the deep MBL phase [52–54]. (g–l) The corresponding distributions of density of states \bar{N}_s versus S , which varies from Gaussian distribution [Eq. (5)] (MBL phase) to a shifted Poisson distribution [Eq. (6)] (volume-law thermalized phase), and finally to the Poisson distribution (deep MBL phase).

tions of product states by variational quantum circuit. Benchmarks are given with the sizes that are far beyond the scope of exact diagonalization. Results on quantum Ising chain in a random field are provided to systematically show the underlying relations between the efficiency of TNVD and the entanglement properties of eigenstates. Typical signs of area-law and volume-law entanglement entropy of eigenstates are suggested, which can assess TNVD efficiency. Our work establishes TNVD as a powerful and scalable diagonalization approach, significantly advancing our ability to diagonalizing large-scale quantum many-body Hamiltonians. The incorporation of VQC in our proposal also lays a clear pathway for future quantum computational approaches to address the Hamiltonians with volume-law-EE eigenstates that are deemed difficult to access by classical methods.

Acknowledgment. PFZ is thankful to Guo-Dong Cheng, Hao Zhu, and Ding-Zu Wang for stimulating discussions. This work was supported in part by Beijing Natural Sci-

ence Foundation (Grant No. 1232025). ACJ is supported by the NSFC (Grant No. 62175169). SJR acknowledges supports from Peng Huanwu Visiting Professor Program, Chinese Academy of Sciences, and Academy for Multidisciplinary Studies, Capital Normal University. The numerical simulations were partially performed on the robotic AI-Scientist platform of Chinese Academy of Sciences.

* Corresponding author. Email: sjran@cnu.edu.cn

- [1] W. Heisenberg, *Zeitschrift für Physik* **49**, 619 (1928).
- [2] H. Bethe, *Zeitschrift für Physik* **71**, 205 (1931).
- [3] J. v. Neumann, *Zeitschrift für Physik* **57**, 30 (1929).
- [4] J. M. Deutsch, *Phys. Rev. A* **43**, 2046 (1991).
- [5] M. Srednicki, *Phys. Rev. E* **50**, 888 (1994).
- [6] H. Lin, J. Gubernatis, H. Gould, and J. Tobochnik, *Computer in Physics* **7**, 400 (1993).
- [7] E. Dagotto, *Rev. Mod. Phys.* **66**, 763 (1994).
- [8] D. J. Luitz, N. Laflorencie, and F. Alet, *Phys. Rev. B* **91**, 081103 (2015).
- [9] S. R. White, *Phys. Rev. Lett.* **69**, 2863 (1992).
- [10] S. R. White and D. A. Huse, *Phys. Rev. B* **48**, 3844 (1993).
- [11] T. Xiang, *Phys. Rev. B* **53**, R10445 (1996).
- [12] V. Khemani, F. Pollmann, and S. L. Sondhi, *Phys. Rev. Lett.* **116**, 247204 (2016).
- [13] X. Yu, D. Pekker, and B. K. Clark, *Phys. Rev. Lett.* **118**, 017201 (2017).
- [14] S.-Y. Zhang, D. Yuan, T. Iadecola, S. Xu, and D.-L. Deng, *Phys. Rev. Lett.* **131**, 020402 (2023).
- [15] F. Pollmann, V. Khemani, J. I. Cirac, and S. L. Sondhi, *Phys. Rev. B* **94**, 041116 (2016).
- [16] T. B. Wahl, A. Pal, and S. H. Simon, *Phys. Rev. X* **7**, 021018 (2017).
- [17] M. Cerezo, A. Arrasmith, R. Babbush, S. C. Benjamin, S. Endo, K. Fujii, J. R. McClean, K. Mitarai, X. Yuan, L. Cincio, and P. J. Coles, *Nature Reviews Physics* **3**, 625 (2021).
- [18] K. Bharti, A. Cervera-Lierta, T. H. Kyaw, T. Haug, S. Alperin-Lea, A. Anand, M. Degroote, H. Heimonen, J. S. Kottmann, T. Menke, W.-K. Mok, S. Sim, L.-C. Kwek, and A. Aspuru-Guzik, *Rev. Mod. Phys.* **94**, 015004 (2022).
- [19] A. Chandran, J. Carrasquilla, I. H. Kim, D. A. Abanin, and G. Vidal, *Phys. Rev. B* **92**, 024201 (2015).
- [20] K. Choo, G. Carleo, N. Regnault, and T. Neupert, *Phys. Rev. Lett.* **121**, 167204 (2018).
- [21] I. Glasser, N. Pancotti, M. August, I. D. Rodriguez, and J. I. Cirac, *Phys. Rev. X* **8**, 011006 (2018).
- [22] V. Vedral and M. B. Plenio, *Phys. Rev. A* **57**, 1619 (1998).
- [23] P. W. Anderson, *Phys. Rev.* **109**, 1492 (1958).
- [24] I. V. Gornyi, A. D. Mirlin, and D. G. Polyakov, *Phys. Rev. Lett.* **95**, 206603 (2005).
- [25] D. Basko, I. Aleiner, and B. Altshuler, *Annals of Physics* **321**, 1126 (2006).
- [26] V. Oganesyan and D. A. Huse, *Phys. Rev. B* **75**, 155111 (2007).
- [27] M. Serbyn, Z. Papić, and D. A. Abanin, *Phys. Rev. Lett.* **111**, 127201 (2013).
- [28] T. Devakul and R. R. P. Singh, *Phys. Rev. Lett.* **115**, 187201 (2015).
- [29] B. Bauer and C. Nayak, *Journal of Statistical Mechanics: Theory and Experiment* **2013**, P09005 (2013).
- [30] J. A. Kjäll, J. H. Bardarson, and F. Pollmann, *Phys. Rev. Lett.* **113**, 107204 (2014).
- [31] M. Friesdorf, A. H. Werner, W. Brown, V. B. Scholz, and J. Eisert, *Phys. Rev. Lett.* **114**, 170505 (2015).
- [32] L. Herviou, S. Bera, and J. H. Bardarson, *Phys. Rev. B* **99**, 134205 (2019).
- [33] J. M. Deutsch, *Phys. Rev. A* **43**, 2046 (1991).
- [34] M. Srednicki, *Phys. Rev. E* **50**, 888 (1994).
- [35] P.-F. Zhou, Y. Lu, J.-H. Wang, and S.-J. Ran, *Phys. Rev. Lett.* **131**, 020403 (2023).
- [36] P.-F. Zhou, R. Hong, and S.-J. Ran, *Phys. Rev. A* **104**, 042601 (2021).
- [37] G. M. Crosswhite and D. Bacon, *Phys. Rev. A* **78**, 012356 (2008).
- [38] F. Fröwis, V. Nebendahl, and W. Dür, *Phys. Rev. A* **81**, 062337 (2010).
- [39] G. Vidal, *Phys. Rev. Lett.* **91**, 147902 (2003).
- [40] G. Vidal, *Phys. Rev. Lett.* **93**, 040502 (2004).
- [41] J. A. Kjäll, J. H. Bardarson, and F. Pollmann, *Phys. Rev. Lett.* **113**, 107204 (2014).
- [42] J. Z. Imbrie, *Phys. Rev. Lett.* **117**, 027201 (2016).
- [43] T. Guhr, A. Müller-Groeling, and H. A. Weidenmüller, *Physics Reports* **299**, 189 (1998).
- [44] Y. Y. Atas, E. Bogomolny, O. Giraud, and G. Roux, *Phys. Rev. Lett.* **110**, 084101 (2013).
- [45] J. Eisert, M. Cramer, and M. B. Plenio, *Rev. Mod. Phys.* **82**, 277 (2010).
- [46] V. Karle, M. Serbyn, and A. A. Michailidis, *Phys. Rev. Lett.* **127**, 060602 (2021).
- [47] M. Serbyn, D. A. Abanin, and Z. Papić, *Nature Physics* **17**, 675 (2021).
- [48] D. Banerjee and A. Sen, *Phys. Rev. Lett.* **126**, 220601 (2021).
- [49] V. Khemani, S. P. Lim, D. N. Sheng, and D. A. Huse, *Phys. Rev. X* **7**, 021013 (2017).
- [50] S. Mohapatra, S. Moudgalya, and A. C. Balram, *Phys. Rev. Lett.* **134**, 210403 (2025).
- [51] A. Pal and D. A. Huse, *Phys. Rev. B* **82**, 174411 (2010).
- [52] E. Baygan, S. P. Lim, and D. N. Sheng, *Phys. Rev. B* **92**, 195153 (2015).
- [53] S. P. Lim and D. N. Sheng, *Phys. Rev. B* **94**, 045111 (2016).
- [54] D. J. Luitz, *Phys. Rev. B* **93**, 134201 (2016).
- [55] M. Iversen and A. E. B. Nielsen, *Phys. Rev. B* **107**, 205140 (2023).
- [56] Q. Chen and Z. Zhu, *Phys. Rev. B* **109**, 014212 (2024).